

# Synthesizing Strong-Coupling Kohn-Luttinger Superconductivity in 2D Van der Waals materials

Shi-Cong Mo<sup>1</sup>, Hongyi Yu<sup>2</sup>, Wéi Wú<sup>1,\*</sup>

<sup>1</sup> School of Physics, Sun Yat-sen University, Guangzhou, Guangdong 510275, China

<sup>2</sup> Guangdong Provincial Key Laboratory of Quantum Metrology and Sensing,

School of Physics and Astronomy, Sun Yat-Sen University (Zhuhai Campus), Zhuhai 519082, China

(Dated: January 21, 2026)

The Kohn-Luttinger (KL) mechanism of pairing, which describes superconductivity emergent from repulsive interactions, typically yields Cooper pairs at high angular-momentum ( $\ell > 0$ ) and extremely low transition temperatures ( $T_c$ ). Here, we reveal an inter-layer s-wave ( $\ell = 0$ ) KL superconductivity with greatly elevated  $T_c$  in a multi-layer Hubbard model, which prototypes stacked two-dimensional (2D) electrons in layered van der Waals materials. By employing determinant quantum Monte Carlo and dynamical mean-field theory simulations, we show that a strong pairing attraction  $V^*$ , without the mediation of collective modes, can emerge between inter-layer electrons in the system. As inter-layer repulsion  $U$  increases,  $V^*$  evolves from a conventional KL relation of  $V^* \propto -U^2$ , to a linear strong-coupling scaling of  $V^* \propto -U$ , resulting in enhanced superconductivity at large  $U$ . This strong-coupling KL pairing is robust against changes in lattice geometries and dimensionalities, and it can persist, in the presence of a large remnant Coulomb repulsion  $U^*$  between pairing electrons. Using *ab initio* calculations, we propose a few 2D layered van der Waals materials that can potentially realize and control this unconventional superconductivity.

*Introduction-* Van der Waals (VdW) materials hosting two-dimensional electrons have emerged as versatile platforms for engineering and studying many exotic correlated phases of matter, including quantum Hall states [1–3], correlated Mott insulating states [4–7], excitonic insulators [8–10], and superconductivity [11–18]. This field is rapidly advancing due to the unparalleled electrical tunability, broad material palette, and moiré engineering capabilities of VdW materials [19], which continue to promise the discovery of new quantum phases.

On the other hand, in condensed matter physics, the discovering and understanding of new mechanisms of unconventional superconductivity [20–35], *i.e.*, in which electron pairing arises sans an electron-phonon-coupling (EPC) origin, have been one of the central research topics. The magnetic-correlation mediated superconductivity (SC) that relevant to cuprates [36–39], iron-based [40, 41], and nickelates [42–45] superconductors marks such an example. Another prominent theoretical paradigm of unconventional SC is the Kohn-Luttinger (KL) superconductivity in metals, where overscreened Coulomb interactions can induce Cooper pairs at high angular-momenta ( $\ell > 0$ ) [46, 47]. Despite its long-standing theoretical proposal, direct experimental evidence for KL SC remains elusive. Recent studies suggest that SC in graphene systems [48–50], and monolayer NbSe<sub>2</sub> [15] could potentially be explained within the KL framework.

In their original proposal, Kohn and Luttinger demonstrated that electron pairing can occur in metals without involving EPC, with  $T_c/T_F \sim \exp[-(2\ell)^4]$  at large  $\ell$ , where  $T_F$  is the Fermi temperature [46]. While such pairing could, in principle, lead to SC, the exponentially suppressed  $T_c$  makes experimental observation challenging. Subsequent theoretical studies have suggested that

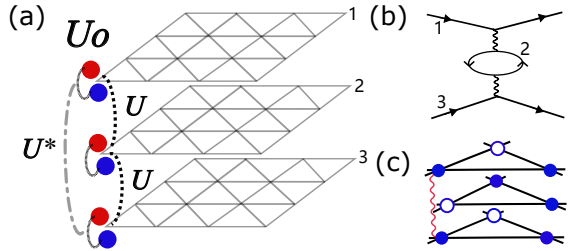


FIG. 1. Illustration of the trilayer Hubbard model and KL electron pairing on 2D triangular lattice. (a): AAA-stacking trilayer triangular lattice with spinfull electrons( $N_l = 3$ ,  $N_\sigma = 2$ ). Within a unit cell, different Hubbard terms  $U_{l\sigma,m\sigma'}$  are depicted. Long-range interaction  $U_{mq}(r)$  terms beyond a unit cell are not shown here. (b): One of the Kohn-Luttinger second order Feynman diagrams leading to inter-layer attraction between a pair of electrons residing on the top- and bottom- layer respectively, via the polarization of the middle-layer. (c): A cartoon showing the inter-layer pairing of two electrons (solid dots) in real-space (indicated by wavy line). Here hollow dots denote holes. For clarity, only one spin species is shown.

lattice effects [51, 52], van Hove singularities [47, 53, 54], the presence of multiple Fermi surfaces [55], and quantum geometry [56, 57] may enhance KL SC. In these studies, KL pairing typically favors a  $d$ - wave ( $\ell = 2$ ) [52, 54], or  $p$ - wave ( $\ell = 1$ ) pairing symmetry [47, 50, 52]. There are also studies suggest that for weakly repulsive electrons in a single-band system, pairing with  $\ell < 3$  is unlikely to occur [58]. These conclusions are primarily derived from weak-coupling considerations. The behaviour of KL SC at strong-coupling remains unclear to date.

In this works, we propose that a trilaminar 2D electron system in stacked van der Waals materials, which can be described by multi-layer Hubbard models (see Fig. 1a),

can be utilized to realize an inter-layer  $s-$  wave strong-coupling KL superconductivity. In the strong-coupling regime, where inter-layer Hubbard repulsion  $U$  becomes comparable to electronic bandwidth  $W$  ( $U \sim W$ ), the effective pairing attraction  $V^*$  exhibits a  $V^* \propto -U$  scaling. This behavior contrasts with the conventional weak-coupling KL pairing where  $V^* \propto -U^2$ , and the magnetic-correlation mediated SC in cuprates where  $V^* \propto -1/U$ ,  $U$  are the respective repulsive coupling constants. Such a linearly growing  $V^*$  leads to enhanced KL SC at large  $U$ , which can persists even in the presence of a large Coulomb repulsion  $U^*$  between paired electrons. We further analyse the dependence of this KL SC on electron densities and long-range Coulomb repulsions. Using density functional theory (DFT) and constrained random phase approximation (cRPA) calculations, we identify several candidate 2D layered half-metals and metals, including metal-doped phosphorene and transition-metal halides [59, 60], as potential platforms for realizing this strong-coupling KL SC.

*Model and Methods* - We consider a three-layer repulsive Hubbard model as following,

$$\begin{aligned} \mathcal{H} = & -t \sum_{\langle i,j \rangle} \sum_{l\sigma} \left( c_{il\sigma}^\dagger c_{jl\sigma} + c_{jl\sigma}^\dagger c_{il\sigma} \right) \\ & + \sum_{il\sigma} (\epsilon_l - \mu) n_{il\sigma} + \sum_i \sum_{l\sigma \neq m\sigma'} \frac{U_{l\sigma, m\sigma'}}{2} n_{il\sigma} n_{im\sigma'} \\ & + \sum_{i,r,l,m,\sigma,\sigma'} U_{lm}(r) n_{i,l,\sigma} n_{i+r,m,\sigma'} \quad (1) \end{aligned}$$

where  $c_{il\sigma}^\dagger$  ( $c_{il\sigma}$ ) denotes the creation (annihilation) operator for a fermion at unit cell  $i$ , layer  $l$ , and with spin flavor  $\sigma$ . The intra-layer nearest-neighbor hopping amplitude  $t$  will be used as the energy unit throughout the paper ( $t \equiv 1$ ). The electron density  $n_l = \langle n_l \rangle$  in each layer can be tuned by the chemical potential  $\mu$  and site-energies  $\epsilon_l$ . Unless specified, we maintain identical density for all three layers:  $n_1 = n_2 = n_3 = n$ . The Hubbard term  $U_{l\sigma, m\sigma'}$  describes repulsions between two electrons in the same unit cell with layer and spin indices  $(l, \sigma)$ , and  $(m, \sigma')$  respectively,  $(l, \sigma) \neq (m, \sigma')$ ,  $U_{l\sigma, m\sigma'} \geq 0$  in our study.  $U_{mq}(r)$  denotes intra- or inter-layer long-ranged Coulomb repulsions beyond a unit cell. Here, we focus on two cases on 2D triangular lattice: trilayer spinless model ( $N_l = 3, N_\sigma = 1$ ) and trilayer spinfull ( $N_l = 3, N_\sigma = 2$ ) model ( See Fig.1). We consider three major term of Hubbard  $U_{l\sigma, m\sigma'}$ : repulsion between electrons at neighboring layers  $U \equiv U_{1\sigma, 2\sigma'} \equiv U_{2\sigma, 3\sigma'}$ , and  $U^* \equiv U_{1\sigma, 3\sigma'}$  for electrons on the top- and bottom-layer. There are also on-site repulsions  $U_o \equiv U_{l\uparrow, l\downarrow}$  in the spinfull model. The effects of non-local  $U_{lm}(r)$  will be investigated at the end of the work. To solve Eq. 1, we employ determinant quantum Monte Carlo (DQMC) and dynamical mean-field theory (DMFT) [61] approaches.

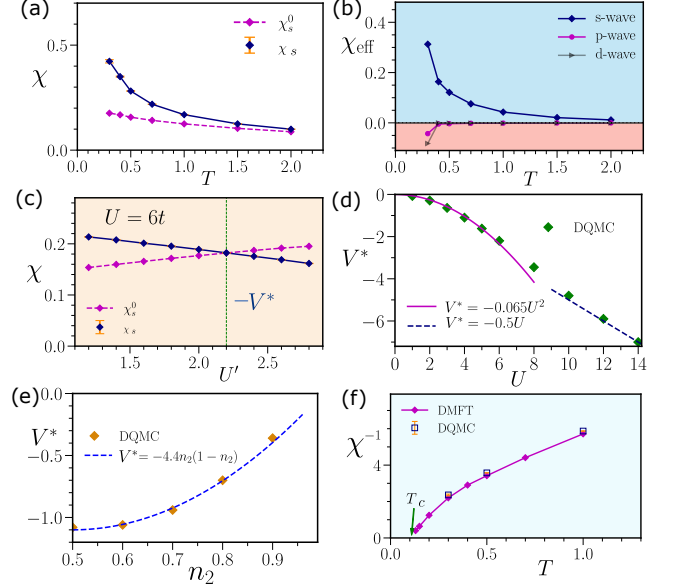


FIG. 2. Pairing susceptibilities  $\chi$  and effective pairing attractions  $V^*$  of the spinless trilayer Hubbard model on 2D triangular lattice from  $6 \times 6 \times 3$  DQMC simulation. (a): Pairing susceptibilities  $\chi_l$  for  $\ell = s-$  wave as a function of temperature  $T$  at  $U = 6, U^* = 0, n_1 = n_2 = n_3 = n = 0.5$ . The bubble contribution  $\chi_s^0$  is shown in dashed line. (b): Effective pairing susceptibilities  $\chi_{\text{eff}} = \chi_l - \chi_{0,l}$  as a function of temperature  $T$ . For  $p-$  and  $d-$  wave,  $\chi_{\text{eff}} < 0$ , denoting these pairing symmetries are disfavored by correlation effects. Other parameters are the same as in (a). (c):  $\chi_s$  and  $\chi_s^0$  as functions of  $U'$  at  $U = 6t, n = 0.5, T = 0.5t$ . The critical  $U'_c$  where  $\chi_s - \chi_s^0 \approx 0$  is used to define the effective pairing attraction  $V^* = -U'_c$ . (d):  $V^*$  as a function of  $U$  at  $n = 0.5, T = 0.5t$ . (e):  $V^*$  as a function of electron density of the middle layer  $n_2$  at  $U = 4, T = 0.5$ . Here  $n_1$  and  $n_3$  are fixed as  $n_1 = n_3 = 0.5$ . (f): Inverse  $s-$  wave pairing susceptibility as a function of temperature  $T$ . Here  $U = 6t, n = 0.6$ .  $\chi^{-1} \rightarrow 0$  is indicated as where  $T$  approaches superconducting transition temperature  $T_c$ . Here  $U^* = 0$  for all plots.

*weak- and strong-coupling limits* We first consider trilayer spinless model with  $U_{12} = U_{23} = U, U_{13} = U^* = 0$ , namely, assuming the Coulomb repulsion  $U^*$  between top- and bottom- layer ( $l = 3$ ) are fully screened off. In weak-coupling limit  $U \ll t$ , the second order KL Feynman diagrams give rise to an inter-layer attraction between top- and bottom- layer (within a unit cell), via the polarization of the middle-layer ( $l = 2$ ), see Fig. 1b and Fig. 1c. In the high temperature limit, this effective attraction  $V_{\text{eff}}$  scales like (see Appendix),

$$V_{\text{eff}} \propto -U^2 n_2 (1 - n_2) \quad (2)$$

where  $n_2$  is the electron filling in the middle-layer. In the large  $U/t \gg 1$  limit at half-filling, to avoid repulsion between electrons (holes) on neighbouring layers, if the top- and bottom- layer are occupied by a pair of electrons (holes), the middle-layer will be occupied by a hole (electron). This occupation configuration has an energy

gain being of the order of  $U$ , hence generating an effective attraction  $V_{\text{eff}}$  between top- and bottom- layer electrons,

$$V_{\text{eff}} \propto -U. \quad (3)$$

see Fig. 1c and Appendix. Therefore, for both weak-coupling and strong-coupling cases, effective attraction between top- and bottom- layer electrons can be generated from the many-body effects of inter-layer repulsion  $U$ .

**DQMC result** - Now we use the numerical exact DQMC to study the spinless model on 2D triangular lattices with  $U_{12} = U_{23} = U, U_{13} = U^* = 0$ . In Fig. 2a, we present DQMC result on the pairing susceptibility  $\chi = \chi_{\ell}^{(l,m)}$  (see Appendix) for electron pairs on the top- and bottom-layer ( $l = 1, m = 3$ ) with  $\ell$ -wave pairing symmetry. In Fig. 2a,  $\chi_s^{(1,3)}$  is plotted for  $\ell = s$  wave as a function of temperature  $T$  (solid line) at  $U = 6, n = 0.5$ , where one can see that  $\chi_s^{(1,3)}$  grows rapidly as  $T$  decreases. The sign problem prevents DQMC from approaching the BKT temperature  $T_{BKT}$  for a diverging pairing susceptibility  $\chi$ . A pragmatic approach to tackle the pairing tendency in DQMC is to estimate the effective pairing  $\chi_{\text{eff}} = \chi - \chi_0$ , where  $\chi$  and  $\chi_0$  are respectively the full pairing susceptibility and bubble contribution. The sign of  $\chi_{\text{eff}}$  reflects whether the vertex corrections, *i.e.*, the interaction effects beyond single-particle level, enhance superconductivity ( $\chi_{\text{eff}} > 0$ ) or suppress superconductivity ( $\chi_{\text{eff}} < 0$ ). Fig. 2a and Fig. 2b suggests that the  $s$ -wave pairing are favoured by correlation effects as  $\chi_{\text{eff}} > 0$ , whereas the  $p$ - and  $d$ - wave pair as disfavored since  $\chi_{\text{eff}} < 0$  for them. We have also considered other pairing correlations, such as the  $s-p-d$ - wave pairings between the top- and middle- layers [ $(l, m) = (1, 2)$ ], where they are all disfavored (data not shown).

To quantify the Kohn-Luttinger (KL) pairing mechanism, we introduce an effective attraction strength,  $V^*$  to describe the attraction between two pairing electrons. This quantity is defined by probing the system's response to pair-breaking repulsion. Specifically, we calculate  $\chi_{\text{eff}}$  for  $s$ - wave pairing between top- and bottom- layer electrons while introducing an explicit interlayer repulsion  $U'$  between them. For  $U' = 0$ , we observe  $\chi_{\text{eff}} > 0$ , indicative of favored pairing, like shown in Fig. 2b. Increasing  $U'$  suppresses  $\chi_{\text{eff}}$ , and we can identify a critical  $U'_c$  where  $\chi_{\text{eff}} \approx 0$ . We then define the effective attraction  $V^*$  as  $V^* = -U'_c$ , as shown in Fig. 2c. This quantity measures the binding strength between two electrons opposing the pair-breaking repulsion. As shown in Fig. 2d,  $V^*$  as a function of  $U$  follows a quadratic dependence  $V^* \propto U^2$  for  $U < 5t$ , consistent with the conventional KL theory [46, 62].

For larger  $U > 5t$ , the quadratic KL relation no longer holds,  $V^*$  gradually transits to a new linear scaling,  $V^* \propto -U$ , underscoring the fundamental difference between KL pairing at strong-coupling and the conventional

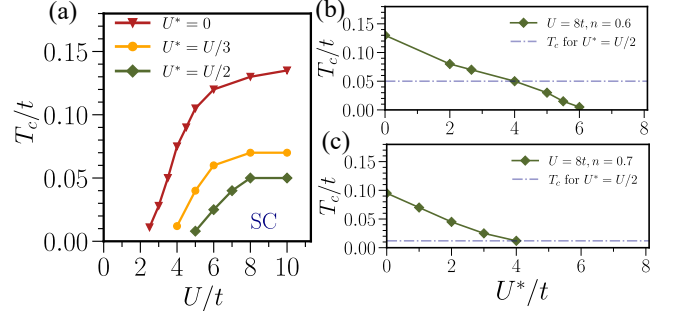


FIG. 3. Superconducting transition temperature  $T_c$  from DMFT calculations. (a)  $T_c$  as a function of  $U$  at  $n_1 = n_2 = n_3 = 0.6$  for a few different  $U^*$ . (b)  $T_c$  as a function of  $U^*$  at  $U = 8t$  at  $n = 0.6$  (20% electron doping). (c) Same as (b) but at  $n = 0.7$  (40% electron doping). In (b) and (c) The values of  $T_c$  at  $U^* = U/2 = 4t$  is marked out by dashed lines.

KL SC (dashed line in Fig. 2d). Fig. 2e shows the density dependence of  $V^*$  at  $U = 6, T = 0.5$ , where one sees that the relation  $V^* \propto n_e^{(2)}(1 - n_e^{(2)})$  is also nicely followed. From above result, we learn that in both weak-coupling and strong-coupling limits, DQMC result of  $V^*$  agrees well with our analytic analysis on  $V_{\text{eff}}$  in Eq. 6 and Eq. 7. In essence, the overall growing tendency of  $V^*$  with  $U$  suggests that one can keep increasing inter-layer Hubbard repulsion  $U$  to realize a larger effective attraction  $V^*$  between electrons, hence potentially a higher transition temperature  $T_c$  for SC.

**SC instability**- We now use CDMFT to compute the superconducting  $T_c$  at small temperatures.  $T_c$  is identified as the temperature where pairing susceptibility  $\chi$  diverges in DMFT. In Fig. 2f, we plot the inverse of  $s$ -wave pairing susceptibility,  $\chi^{-1}$  as a function of  $T$  at  $U = 6, n = 0.6$ . DQMC data available at high temperatures are also presented, where excellent agreement between DMFT and DQMC results can be seen. Extrapolating DMFT result of  $\chi^{-1}$  to zero,  $\chi^{-1} \rightarrow 0$ , we obtain a superconducting  $T_c \approx 0.12t$  for the given parameters in this plot. Repeating the calculations of  $T_c$  for different  $U$ , the  $U$ -dependence of  $T_c$  is obtained in Fig. 3a. In this plot, one sees that superconducting  $T_c$  (triangles) grows with  $U$  in a broad range of  $U$ , in consistent with the DQMC result ( $V^*$  versus  $U$  in Fig. 2d). Specifically, escalated  $T_c \gtrsim 0.12t$  can be found when  $U$  is in the range of  $U \sim (6t, 10t)$ , namely, when  $U$  becomes comparable with bandwidth  $W$  ( $W = 9t$  for 2D triangular lattice), KL SC can be greatly enhanced. For comparison, in the magnetic-fluctuation mediated SC in the single-band 2D Hubbard model, the optimal superconducting  $T_c$  obtained by CDMFT is commonly less than  $T_c \lesssim 0.05t$  [39, 63, 64]. This means that in terms of the reduced pairing energy scale,  $T_c/t$ , the strong-coupling KL SC in the trilayer Hubbard model has an intrinsically stronger pairing force than that in the magnetic-fluctuation mediated SC in Hubbard model.

Furthermore, the nonzero  $U^*$  cases shown in Fig. 3a (dots and diamonds) suggest that in the presence of significant remnant Coulomb repulsion ( $U^* = U/3, U/2$ ) between paired electrons, large superconducting  $T_c$  can be still maintained. In Fig. 3b and Fig. 3c,  $T_c$  as a function of  $U^*$  are shown at  $n = 0.6, 0.7$  respectively (for fixed  $U = 8t$ ), where finite  $T_c$  can be found even when  $U^* \geq U/2$ . Specifically, for the  $n = 0.6$  case, an enhanced  $T_c \approx 0.05t$  is found at  $U = 8t, U^* = 4t$ . This means that in the large screening length limit  $\lambda_{TF} \rightarrow \infty$  along c-axis, *i.e.*, when Coulomb potential in the vertical direction becomes,  $U(r_z) \propto \frac{e^{-r_z/\lambda_{TF}}}{r_z} \sim \frac{1}{r_z}$ , (thus  $U^* \sim U/2$  if layer distances  $d_{12} = d_{23}$ ), the strong-coupling KL SC can still survive. This finding obviously lie beyond the expectation of high-temperature DQMC results presented in Fig. 2d, where  $V^* \sim -U/2$  for large  $U$ . In a purely static picture, a condition of  $U^* \gtrsim U/2$  leads to a net repulsion between top- and bottom-layer electrons [*i.e.*,  $(U^* + V^*) \gtrsim 0$ ], thereby severely inhibiting pairing between them. Hence, the persistence of a high  $T_c$  under  $U^* \gtrsim U/2$  suggests that the retardation part of pairing force may play a role at low temperatures (see discussions in Appendix). A further key point to emphasize is the sizeable  $T_c$  up to a filling of  $n = 0.7$  (40% electron doping), as evidenced in Fig. 3c. This presents a clear difference with the case in Hubbard model for cuprates [63], where SC, induced by magnetic correlations, rapidly vanishes beyond  $p \lesssim 30\%$  for hole-doping and  $p \lesssim 20\%$  for electron-doping. This distinctness is rooted in the “pairing glue”: whereas SC in cuprates relies on the collective spin fluctuations [38] that are suppressed as  $n \gg 0.5$  or  $n \ll 0.5$ , the strong-coupling KL SC identified here does

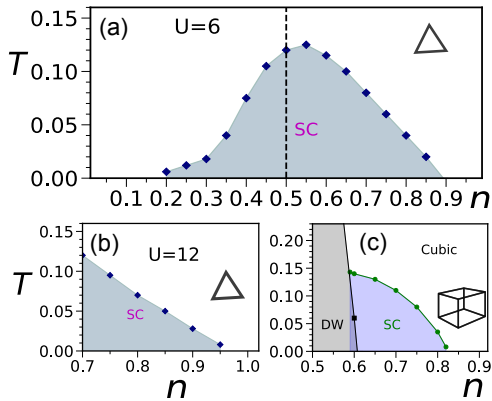


FIG. 4. Phase diagrams showing superconducting instability (SC) and density wave (DW) instability. (a) Superconducting transition temperature  $T_c$  as a function of electron density  $n$  on the 2D triangular lattice at  $U = 6$ . (b) Same as (a) but at  $U = 12$ . (c) Density wave and superconducting transition temperatures as a function of electron density  $n$  on the 3D cubic lattice at  $U = 10$ . Here for all three cases  $n_1 = n_2 = n_3 = n$ . The repulsion between layer- (spin flavor-) 1 and layer- (spin flavor-) 3,  $U_{13} = U' = 0$ .

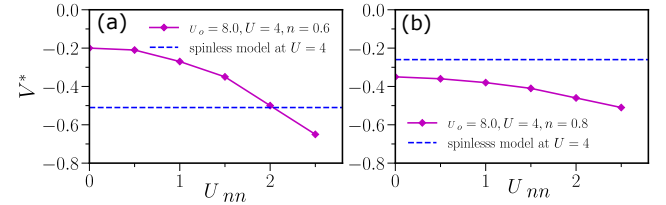


FIG. 5. Effective pairing attraction  $V^*$  as a function long-range Coulomb repulsion  $U_{nn}$  for spinless and spinfull models on 2d Triangular lattice at  $U = 4, U_o = 8, U' = 0, T = 1.0$ .  $U_{nn}$  denotes repulsion between intra-layer nearest-neighbouring sites,  $U_{nn} \equiv U_{ll}(|r| = 1)$ .

not involve any intermediate collective modes, thus ensuring robustness across a broad range of  $n$ .

*The phase diagrams* - Fig. 4a presents a superconducting phase diagram showing  $T_c$  as a function of electron density  $n$  at  $U = 6, U^* = 0$  for the spinless model on 2D triangular lattice from nearly empty ( $n \sim 0.2$ ) to nearly full-filled ( $n \sim 0.9$ ) at  $U = 6t, U^* = 0$ . One sees that  $T_c$  is maximized as  $n$  being close to half-filling, in agreement with the  $V^*$  versus  $n$  tendency in DQMC (Fig. 2e). Again, here we find KL SC instability in an extremely large range of  $n$ . Increasing Hubbard repulsion to  $U = 12t$  can even further expand the SC regime. For instance, on the electron doped side, KL SC extends to  $n_c \gtrsim 0.95$  as  $T \rightarrow 0$  (Fig. 4b).

Near half-filling, we find strong density fluctuations in DMFT calculations despite no stable long-range ordered state found on the triangular lattice. For comparison, in Fig. 4c, we present a similar phase diagram for the non-frustrated cubic lattice (where the layer index  $l$  now can be understood as a pseudo-spin index). At half-filling ( $n = 0.5$ ), this system indeed develops a density wave (DW) phase (Fig. 4c, see also Appendix). This long-range DW instability competes with SC order, which can be destroyed by doping electrons (holes). As DW order vanishes (e.g.  $n \gtrsim 0.6$  in Fig. 4c), SC instability emerges. Further increasing  $n$  leads to the decreasing of superconducting  $T_c$ , similar to the triangular lattice result. This finding demonstrates that strong-coupling KL SC is robust against changes in lattice geometry (Cubic V.S. Triangular) and dimensionality (3D V.S. 2D).

*Spinful model and effects of  $U_{lm}(r)$*  - In the spinful model of Eq. 1, twofold competing effects can influence interlayer KL pairing relative to the spinless case: (1) the extra spin degree of freedom in the middle layer can enhance pairing by offering an additional polarization channel mediating attraction; (2) on the other hand, strong on-site repulsion  $U_o$  between opposite-spin electrons induces local electron-hole pairs (*i.e.*, local moments), which is detrimental to interlayer electron-electron pairing. How  $T_c$  of KL SC changes in the spinful model is therefore determined by the balance between these two opposing mechanisms.

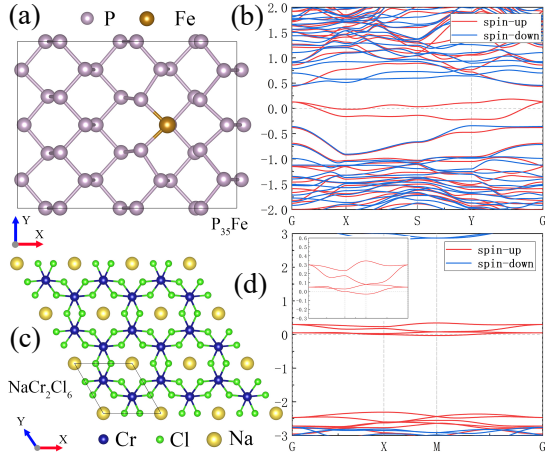


FIG. 6. Crystal and band structure of the Iron-doped Phosphorene and decorated transition metal halides  $CrCl_3$ . (a) Top view of the crystal structure of  $P_{35}Fe$ . (b) Energy band structure of  $P_{35}Fe$ . (c) Crystal structure of Na-absorbed  $CrCl_3$ ,  $NaCr_2Cl_6$ . (d) Energy band structure of  $NaCr_2Cl_6$ .

We examine the influence of both the on-site  $U_o$  and long-range  $U_{lm}(r)$  on  $V^*$  in Fig. 5. For  $U_{lm}(r)$ , as a concrete example, we consider its intra-layer nearest-neighbor (NN) component, denoted as  $U_{nn} \equiv U_{ll}(|r|=1)$ . Fig. 5a shows that at  $U_{nn}=0$ , the spinfull model (at  $U_o=8t, U=4t$ ) yields a significantly smaller effective attraction  $V^*$  compared to the corresponding spinless model (dashed line, without  $U_o$ , and  $U=4t, U_{nn}=0$ ), confirming that  $U_o$  suppresses KL pairing. As  $U_{nn}$  increases,  $V^*$  grows in the spinful case, and it exceeds the spinless value once  $U_{nn} > 2t$ . This finding indicates that  $U_{nn}$  in fact boosts KL pairing. This is because long-range Coulomb repulsions generally promotes charge density wave (CDW) fluctuations, which intrinsically suppresses the detrimental local moment effect induced by  $U_o$ . At a higher filling  $n=0.8$  (Fig. 5b),  $V^*$  is also seen enhanced by  $U_{nn}$ . In this case, the spinful model already gives a larger  $V^*$  than its spinless counterpart even at  $U_{nn}=0$ . This is expected, because, far away from half-filling ( $n \gg 0.5$ ), local moments are suppressed by doping, thus the additional polarization channel effect in the spinful model becomes predominant, which results in a large  $V^*$ .

*Realization of strong-coupling KL pairing-* As demonstrated above, enhanced KL pairing can be achieved in a trilayer structure of 2D electrons when interlayer repulsion  $U$  is comparable to the bandwidth  $W$ . In 2D van der Waals layered materials, the interlayer interaction can reach  $U \lesssim 0.5eV$  (see Appendix and Ref. [65]). To satisfy the strong-coupling condition  $U \gtrsim W$ , a narrow electronic bandwidth is therefore needed,  $W \lesssim 0.5eV$ . Through density functional theory (DFT) and constrained random-phase approximation (cRPA) calculations, we have identified several atom-

ically thin two-dimensional half-metals that can effectively realize the trilayer spinless Hubbard model fulfilling  $W \lesssim U$ . Examples include iron-doped phosphorene ( $FeP_{35}$ ), with  $W \sim 0.37eV$  and  $U \sim 0.15eV$ , and sodium-adsorbed transition-metal trihalides such as  $NaCr_2Cl_6$ , where  $W \sim 0.087eV$  and  $U \sim 0.3eV$  (see Fig. 6 and Appendix). Finally, recent advances in engineering artificial two-dimensional electron lattices in semiconductor heterostructures have achieved bandwidths of only a few meV [66], offering another promising platform for realizing strong KL superconductivity.

*Discussion and conclusion -* We have proposed that multi-layered 2D electron systems can be engineered to realize a novel emergent quantum many-body state: strong-coupling KL superconductivity. A key advantage of our proposal lies in the large pairing energy scale of the strong-coupling KL SC, which does not need an intermediate collective mode [34, 35] to mediate the pairing. As a result, it exhibits robustness against variations in lattice geometry and dimensionality, and can endure a large remnant Coulomb repulsion  $U^*$  between pairing electrons. These advantages allow substantial flexibility to control the pairing by tuning sample thickness, dielectric environment or interlayer distance in VdW materials. Although our low-temperature DMFT calculations of  $T_c$  are restricted to the spinless model for half-metals due to numerical challenges, the DQMC results do suggest that the spinful model (for normal 2D metals) can, under proper conditions, host an even stronger effective pairing attraction  $V^*$ .

In summary, we have demonstrated the emergence of a robust, strong-coupling inter-layer  $s$ -wave Kohn-Luttinger superconducting state in multi-layer Hubbard models prototyping stacked 2D electron systems. Our *ab initio* calculations identify a few candidate materials capable of realizing this novel state, indicating that 2D van der Waals materials can also constitute a versatile platform for designing and manipulating unconventional superconductivity.

*Acknowledgment* We are grateful to Fadi Sun for useful discussions. This work is supported by the National Natural Science Foundation of China (Grants No.12274472, No. 12494594). We also thank the support from the Research Center for Magnetoelectric Physics of Guangdong Province (Grants No. 2024B0303390001) and Guangdong Provincial Quantum Science Strategic Initiative (Grant No. GDZX2401010).

\* Corresponding author: wuwei69@mail.sysu.edu.cn

- [1] M. Serlin, C. Tschirhart, H. Polshyn, Y. Zhang, J. Zhu, K. Watanabe, T. Taniguchi, L. Balents, and A. Young, Intrinsic quantized anomalous hall effect in a moiré heterostructure, *Science* **367**, 900 (2020).
- [2] Y.-M. Xie, C.-P. Zhang, J.-X. Hu, K. F. Mak, and

K. Law, Valley-polarized quantum anomalous hall state in moiré mote 2/wse 2 heterobilayers, *Physical Review Letters* **128**, 026402 (2022).

[3] F. Xu, Z. Sun, T. Jia, C. Liu, C. Xu, C. Li, Y. Gu, K. Watanabe, T. Taniguchi, B. Tong, J. Jia, Z. Shi, S. Jiang, Y. Zhang, X. Liu, and T. Li, Observation of integer and fractional quantum anomalous hall effects in twisted bilayer mote<sub>2</sub>, *Phys. Rev. X* **13**, 031037 (2023).

[4] Y. Cao, V. Fatemi, A. Demir, S. Fang, S. L. Tomarken, J. Y. Luo, J. D. Sanchez-Yamagishi, K. Watanabe, T. Taniguchi, E. Kaxiras, *et al.*, Correlated insulator behaviour at half-filling in magic-angle graphene superlattices, *Nature* **556**, 80 (2018).

[5] Y. Xu, S. Liu, D. A. Rhodes, K. Watanabe, T. Taniguchi, J. Hone, V. Elser, K. F. Mak, and J. Shan, Correlated insulating states at fractional fillings of moiré superlattices, *Nature* **587**, 214 (2020).

[6] E. C. Regan, D. Wang, C. Jin, M. I. Bakti Utama, B. Gao, X. Wei, S. Zhao, W. Zhao, Z. Zhang, K. Yumigeta, *et al.*, Mott and generalized wigner crystal states in wse2/ws2 moiré superlattices, *Nature* **579**, 359 (2020).

[7] X. Huang, T. Wang, S. Miao, C. Wang, Z. Li, Z. Lian, T. Taniguchi, K. Watanabe, S. Okamoto, D. Xiao, *et al.*, Correlated insulating states at fractional fillings of the ws2/wse2 moiré lattice, *Nature Physics* **17**, 715 (2021).

[8] M. Xie, H. Pan, F. Wu, and S. Das Sarma, Nematic excitonic insulator in transition metal dichalcogenide moiré heterobilayers, *Phys. Rev. Lett.* **131**, 046402 (2023).

[9] P. X. Nguyen, L. Ma, R. Chaturvedi, K. Watanabe, T. Taniguchi, J. Shan, and K. F. Mak, Perfect coulomb drag in a dipolar excitonic insulator, *Science* **388**, 274 (2025).

[10] R. Qi, A. Y. Joe, Z. Zhang, J. Xie, Q. Feng, Z. Lu, Z. Wang, T. Taniguchi, K. Watanabe, S. Tongay, *et al.*, Perfect coulomb drag and exciton transport in an excitonic insulator, *Science* **388**, 278 (2025).

[11] Y. Cao, V. Fatemi, S. Fang, K. Watanabe, T. Taniguchi, E. Kaxiras, and P. Jarillo-Herrero, Unconventional superconductivity in magic-angle graphene superlattices, *Nature* **556**, 43 (2018).

[12] X. Lu, P. Stepanov, W. Yang, M. Xie, M. A. Aamir, I. Das, C. Urgell, K. Watanabe, T. Taniguchi, G. Zhang, *et al.*, Superconductors, orbital magnets and correlated states in magic-angle bilayer graphene, *Nature* **574**, 653 (2019).

[13] M. Yankowitz, S. Chen, H. Polshyn, Y. Zhang, K. Watanabe, T. Taniguchi, D. Graf, A. F. Young, and C. R. Dean, Tuning superconductivity in twisted bilayer graphene, *Science* **363**, 1059 (2019).

[14] X. Xi, Z. Wang, W. Zhao, J.-H. Park, K. T. Law, H. Berger, L. Forró, J. Shan, and K. F. Mak, Ising pairing in superconducting nbse 2 atomic layers, *Nature Physics* **12**, 139 (2016).

[15] J. Siegl, A. Bleibaum, W. Wan, M. Kurpas, J. Schliemann, M. M. Ugeda, M. Marganska, and M. Grifoni, Friedel oscillations and chiral superconductivity in monolayer nbse2, *Nature Communications* **16**, 8228 (2025).

[16] Y. Xia, Z. Han, K. Watanabe, T. Taniguchi, J. Shan, and K. F. Mak, Superconductivity in twisted bilayer wse2, *Nature* **637**, 833 (2025).

[17] Y. Guo, J. Pack, J. Swann, L. Holtzman, M. Cothrine, K. Watanabe, T. Taniguchi, D. G. Mandrus, K. Barmak, J. Hone, *et al.*, Superconductivity in 5.0° twisted bilayer wse2, *Nature* **637**, 839 (2025).

[18] A. Ghazaryan, T. Holder, M. Serbyn, and E. Berg, Unconventional superconductivity in systems with annular fermi surfaces: Application to rhombohedral trilayer graphene, *Phys. Rev. Lett.* **127**, 247001 (2021).

[19] K. S. Novoselov, A. Mishchenko, A. Carvalho, and A. Castro Neto, 2d materials and van der waals heterostructures, *Science* **353**, aac9439 (2016).

[20] J. G. Bednorz and K. A. Müller, Possible high t c superconductivity in the ba- la- cu- o system, *Zeitschrift für Physik B Condensed Matter* **64**, 189 (1986).

[21] H. Sun, M. Huo, X. Hu, J. Li, Z. Liu, Y. Han, L. Tang, Z. Mao, P. Yang, B. Wang, *et al.*, Signatures of superconductivity near 80 k in a nickelate under high pressure, *Nature* **621**, 493 (2023).

[22] G. Kotliar and J. Liu, Superexchange mechanism and d-wave superconductivity, *Phys. Rev. B* **38**, 5142 (1988).

[23] F.-C. Zhang, C. Gros, T. M. Rice, and H. Shiba, A renormalised hamiltonian approach to a resonant valence bond wavefunction, *Superconductor Science and Technology* **1**, 36 (1988).

[24] T. Moriya, Y. Takahashi, and K. Ueda, Antiferromagnetic spin fluctuations and superconductivity in two-dimensional metals—a possible model for high tc oxides, *Journal of the Physical Society of Japan* **59**, 2905 (1990).

[25] V. Emery and S. Kivelson, Importance of phase fluctuations in superconductors with small superfluid density, *Nature* **374**, 434 (1995).

[26] P. A. Lee, N. Nagaosa, and X.-G. Wen, Doping a Mott insulator: Physics of high-temperature superconductivity, *Rev. Mod. Phys.* **78**, 17 (2006).

[27] M. R. Norman, The challenge of unconventional superconductivity, *Science* **332**, 196 (2011).

[28] V. Crépel and L. Fu, New mechanism and exact theory of superconductivity from strong repulsive interaction, *Science Advances* **7**, eabh2233 (2021).

[29] M. T. Schmid, J.-B. Morée, R. Kaneko, Y. Yamaji, and M. Imada, Superconductivity studied by solving ab initio low-energy effective hamiltonians for carrier doped cacuo<sub>2</sub>, bi<sub>2</sub>sr<sub>2</sub>cuo<sub>6</sub>, bi<sub>2</sub>sr<sub>2</sub>cacu<sub>2</sub>o<sub>8</sub>, and hgba<sub>2</sub>cuo<sub>4</sub>, *Phys. Rev. X* **13**, 041036 (2023).

[30] M. Christos, Z.-X. Luo, H. Shackleton, Y.-H. Zhang, M. S. Scheurer, and S. Sachdev, A model of d-wave superconductivity, antiferromagnetism, and charge order on the square lattice, *Proceedings of the National Academy of Sciences* **120**, e2302701120 (2023).

[31] V. Crépel, D. Guerci, J. Cano, J. H. Pixley, and A. Millis, Topological superconductivity in doped magnetic moiré semiconductors, *Phys. Rev. Lett.* **131**, 056001 (2023).

[32] A. Kumar, A. S. Patri, and T. Senthil, Unconventional superconductivity mediated by exciton density wave fluctuations, *arXiv preprint arXiv:2410.09148* (2024).

[33] Z. Dong and P. A. Lee, A controlled expansion for pairing in a polarized band with strong repulsion (2025), *arXiv:2503.11079 [cond-mat.supr-con]*.

[34] J. von Milczewski, X. Chen, A. Imamoglu, and R. Schmidt, Superconductivity induced by strong electron-exciton coupling in doped atomically thin semiconductor heterostructures, *Physical Review Letters* **133**, 226903 (2024).

[35] C. Zerba, C. Kuhlenkamp, A. Imamoglu, and M. Knap, Realizing topological superconductivity in tunable bose-fermi mixtures with transition metal dichalcogenide heterostructures, *Physical Review Letters* **133**, 056902 (2024).

[36] T. A. Maier, D. Poilblanc, and D. Scalapino, Dynamics of the pairing interaction in the hubbard and t- j models of high-temperature superconductors, *Physical review letters* **100**, 237001 (2008).

[37] B. Kyung, D. Sénéchal, and A.-M. Tremblay, Pairing dynamics in strongly correlated superconductivity, *Physical Review B* **80**, 205109 (2009).

[38] X. Dong, E. Gull, and A. J. Millis, Quantifying the role of antiferromagnetic fluctuations in the superconductivity of the doped hubbard model, *Nature Physics* **18**, 1293 (2022).

[39] J. Liu, D.-X. Yao, and W. Wu, Interplay between the pseudogap and superconductivity in doped mott insulators: a cluster dynamical mean-field theory study, *Chinese Physics Letters* **42**, 080711 (2025).

[40] A. V. Chubukov, D. V. Efremov, and I. Eremin, Magnetism, superconductivity, and pairing symmetry in iron-based superconductors, *Phys. Rev. B* **78**, 134512 (2008).

[41] F. Wang and D.-H. Lee, The electron-pairing mechanism of iron-based superconductors, *Science* **332**, 200 (2011).

[42] S. Middey, J. Chakhalian, P. Mahadevan, J. Freeland, A. J. Millis, and D. Sarma, Physics of ultrathin films and heterostructures of rare-earth nickelates, *Annual Review of Materials Research* **46**, 305 (2016).

[43] Y. Nomura and R. Arita, Superconductivity in infinite-layer nickelates, *Reports on Progress in Physics* **85**, 052501 (2022).

[44] W. Wú, Z. Luo, D.-X. Yao, and M. Wang, Superexchange and charge transfer in the nickelate superconductor  $La_3Ni_2O_7$  under pressure, *Science China Physics, Mechanics & Astronomy* **67**, 117402 (2024).

[45] S.-c. Mo, Y.-y. Zheng, and W. Wú, Intertwined electron pairing in the bilayer two-orbital kanamori-hubbard model: a unified picture of two superconductivities in  $La_3Ni_2O_7$ , *arXiv preprint arXiv:2508.04554* (2025).

[46] W. Kohn and J. Luttinger, New mechanism for superconductivity, *Physical Review Letters* **15**, 524 (1965).

[47] M. Y. Kagan, V. Val'kov, V. Mitskan, and M. Kovalchuk, The kohn-luttinger effect and anomalous pairing in new superconducting systems and graphene, *Journal of Experimental and Theoretical Physics* **118**, 995 (2014).

[48] J. Gonzalez and T. Stauber, Kohn-luttinger superconductivity in twisted bilayer graphene, *Physical review letters* **122**, 026801 (2019).

[49] T. Cea and F. Guinea, Coulomb interaction, phonons, and superconductivity in twisted bilayer graphene, *Proceedings of the National Academy of Sciences* **118**, e2107874118 (2021).

[50] M. Geier, M. Davydova, and L. Fu, Chiral and topological superconductivity in isospin polarized multilayer graphene, *Nature Communications* (2025).

[51] M. Baranov, A. Chubukov, and M. Yu. Kagan, Superconductivity and superfluidity in fermi systems with repulsive interactions, *International Journal of Modern Physics B* **6**, 2471 (1992).

[52] S. Raghu, S. Kivelson, and D. Scalapino, Superconductivity in the repulsive hubbard model: An asymptotically exact weak-coupling solution, *Physical Review B—Condensed Matter and Materials Physics* **81**, 224505 (2010).

[53] J. Gonzalez, Kohn-luttinger superconductivity in graphene, *Physical Review B—Condensed Matter and Materials Physics* **78**, 205431 (2008).

[54] R. Nandkishore, L. S. Levitov, and A. V. Chubukov, Chiral superconductivity from repulsive interactions in doped graphene, *Nature Physics* **8**, 158 (2012).

[55] A. V. Chubukov and S. A. Kivelson, Superconductivity in engineered two-dimensional electron gases, *Physical Review B* **96**, 174514 (2017).

[56] G. Shavit and J. Alicea, Quantum geometric kohn-luttinger superconductivity, *Physical Review Letters* **134**, 176001 (2025).

[57] A. Jahn and S.-Z. Lin, Enhanced kohn-luttinger superconductivity in geometric bands, *Phys. Rev. B* **113**, 014504 (2026).

[58] A. Alexandrov and V. Kabanov, Unconventional high-temperature superconductivity from repulsive interactions: theoretical constraints, *Physical Review Letters* **106**, 136403 (2011).

[59] C. Chen, W. Ou, K.-M. Yam, S. Xi, X. Zhao, S. Chen, J. Li, P. Lyu, L. Ma, Y. Du, W. Yu, H. Fang, C. Yao, X. Hai, H. Xu, M. J. Koh, S. J. Pennycook, J. Lu, M. Lin, C. Su, C. Zhang, and J. Lu, Zero-valent palladium single-atoms catalysts confined in black phosphorus for efficient semi-hydrogenation, *Advanced Materials* **33**, 2008471 (2021).

[60] B. Liu, M. Köpf, A. N. Abbas, X. Wang, Q. Guo, Y. Jia, F. Xia, R. Weihrich, F. Bachhuber, F. Pielenhofer, H. Wang, R. Dhall, S. B. Cronin, M. Ge, X. Fang, T. Nilges, and C. Zhou, Black arsenic–phosphorus: Layered anisotropic infrared semiconductors with highly tunable compositions and properties, *Advanced Materials* **27**, 4423.

[61] A. Georges, Dynamical mean-field theory of strongly correlated fermion systems and the limit of infinite dimensions, *Reviews of Modern Physics* **68** (1996).

[62] A. T. Rømer, T. A. Maier, A. Kreisel, I. Eremin, P. Hirschfeld, and B. M. Andersen, Pairing in the two-dimensional hubbard model from weak to strong coupling, *Physical Review Research* **2**, 013108 (2020).

[63] L. Fratino, P. Sémon, G. Sordi, and A.-M. Tremblay, An organizing principle for two-dimensional strongly correlated superconductivity, *Scientific reports* **6**, 1 (2016).

[64] T. A. Maier and D. J. Scalapino, Pairfield fluctuations of a 2d hubbard model, *npj Quantum Materials* **4**, 30 (2019).

[65] M. Van der Donk and F. M. Peeters, Interlayer excitons in transition metal dichalcogenide heterostructures, *Phys. Rev. B* **98**, 115104 (2018).

[66] D. Q. Wang, Z. Krix, O. A. Tkachenko, V. A. Tkachenko, C. Chen, I. Farrer, D. A. Ritchie, O. P. Sushkov, A. R. Hamilton, and O. Klochan, *Artificial electrostatic crystals: a new platform for creating correlated quantum states* (2025), *arXiv:2402.12769 [cond-mat.mes-hall]*.

[67] P. Seth, I. Krivenko, M. Ferrero, and O. Parcollet, Triqs/cthyb: A continuous-time quantum monte carlo hybridisation expansion solver for quantum impurity problems, *Computer Physics Communications* **200**, 274 (2016).

[68] O. Parcollet, M. Ferrero, T. Ayral, H. Hafermann, I. Krivenko, L. Messio, and P. Seth, TRIQS: A toolbox for research on interacting quantum systems, *Computer Physics Communications* **196**, 398 (2015), *arXiv:1504.01952*.

[69] G. Kresse and J. Hafner, Ab initio molecular dynamics for liquid metals, *Physical review B* **47**, 558 (1993).

[70] G. Kresse and J. Furthmüller, Efficient iterative schemes

for ab initio total-energy calculations using a plane-wave basis set, *Physical review B* **54**, 11169 (1996).

[71] J. P. Perdew, K. Burke, and M. Ernzerhof, Generalized gradient approximation made simple, *Physical review letters* **77**, 3865 (1996).

[72] J. Shi, G. W. Fernando, Y. Dang, S. L. Suib, and M. Jain, Structural and electronic properties of rare-earth chromites: A computational and experimental study, *Physical Review B* **106**, 165117 (2022).

[73] N. Naveas, R. Pulido, C. Marini, P. Gargiani, J. Hernandez-Montelongo, I. Brito, and M. Manso-Silván, First-principles calculations of magnetite (fe<sub>3</sub>o<sub>4</sub>) above the verwey temperature by using self-consistent dft+ u+ v, *Journal of Chemical Theory and Computation* **19**, 8610 (2023).

[74] A. A. Mostofi, J. R. Yates, G. Pizzi, Y.-S. Lee, I. Souza, D. Vanderbilt, and N. Marzari, An updated version of wannier90: A tool for obtaining maximally-localised wannier functions, *Computer Physics Communications* **185**, 2309 (2014).

[75] N. Marzari, A. A. Mostofi, J. R. Yates, I. Souza, and D. Vanderbilt, Maximally localized wannier functions: Theory and applications, *Reviews of Modern Physics* **84**, 1419 (2012).

[76] Y. Gao, W. Wu, Z. Liu, K. Held, and L. Si, Topotactical hydrogen induced single-band d-wave superconductivity in la 2 nio 4, *Physical Review Letters* **135**, 026002 (2025).

## APPENDIX

### Multi-layer Hubbard model and methods

In the trilayer spinless model with  $U_{12} = U_{23} = U, U_{13} = U^* = 0$ , namely, when the Coulomb repulsions are present only between neighbouring layers. In the weak-coupling limit  $U \ll t$ , the second order KL Feynman diagram contributes an effective attraction between the top and bottom layer electrons, via the polarization of the middle-layer ( $l = 2$ ) electrons [46, 62],

$$V_{KL}(K, K') = \frac{U^2}{N} [\chi_0(K + K') - \chi_0(K - K')] \quad (4)$$

$$\chi_0(q) = \frac{1}{N} \sum_K g_0(K + q) g_0(K) \quad (5)$$

where  $\chi_0(q)$  is the Lindhard function at transfer momentum  $q$ , and  $N$  is the number of unit cells. In the high-

temperature limit, this Kohn-Luttinger interaction introduces an effective attraction  $V^*$  between a pair of electrons located on top- and bottom- layer in a unit cell, which scales like,

$$V^* \propto -U^2 n_2(1 - n_2) \quad (6)$$

where  $n_2$  is the electron filling factor of the middle-layer.

In the large  $U$  limit ( $U/t \gg 1$  or  $U/W \gg 1$ ) at half-filling, to avoid repulsion between electrons (holes) on neighboring layers, the middle-layer tends to be occupied by the opposite carriers of top- and bottom-layer. This occupation configuration will have an energy gain of the order of  $-U$  over the first excited state. To be specific, we consider three layers of intra-layer electron-hole pairs (denoted as  $\bullet - \circ$ ) in the spinless model. There are three different states of most interest to our problem,

$$\begin{aligned} & \frac{\sqrt{2}}{2} \left( \left| \begin{array}{c} \bullet - \circ \\ \circ - \bullet \\ \bullet - \circ \end{array} \right\rangle + \left| \begin{array}{c} \circ - \bullet \\ \bullet - \circ \\ \circ - \bullet \end{array} \right\rangle \right) \quad \textcircled{A} \\ & \frac{1}{2} \left( \left| \begin{array}{c} \circ - \bullet \\ \circ - \bullet \\ \bullet - \circ \end{array} \right\rangle + \left| \begin{array}{c} \circ - \bullet \\ \bullet - \circ \\ \bullet - \circ \end{array} \right\rangle + \left| \begin{array}{c} \bullet - \circ \\ \circ - \bullet \\ \circ - \bullet \end{array} \right\rangle + \left| \begin{array}{c} \bullet - \circ \\ \bullet - \circ \\ \circ - \bullet \end{array} \right\rangle \right) \quad \textcircled{B} \\ & \frac{\sqrt{8}}{8} \left( \left| \begin{array}{c} \circ - \bullet \\ \bullet - \bullet \\ \circ - \circ \end{array} \right\rangle + \left| \begin{array}{c} \bullet - \circ \\ \bullet - \bullet \\ \circ - \circ \end{array} \right\rangle + \left| \begin{array}{c} \circ - \bullet \\ \circ - \circ \\ \bullet - \bullet \end{array} \right\rangle + \left| \begin{array}{c} \bullet - \circ \\ \circ - \circ \\ \bullet - \bullet \end{array} \right\rangle + \textcircled{1} \rightleftharpoons \textcircled{3} \right) \quad \textcircled{C} \end{aligned}$$

In state  $\textcircled{A}$ , electrons can avoid any inter-layer repulsion  $U$  between neighboring layers, thus it becomes the ground state in the large  $U$  limit at half-filling. Obviously, this state is the physical origin where pairing of two electrons emerges on top- and bottom-layer respectively. State  $\textcircled{B}$  is the first excited state, given the total density fluctuation in each layer is forbidden (*i.e.*  $\delta n_l = 0$ ).

This state has an energy gain of  $\Delta E = (U - t)$  relative to the ground state  $\textcircled{A}$ . On the other hand, if the total density fluctuation in layers are allowed, then state  $\textcircled{C}$  becomes the first excited state, which has an energy gain of  $\Delta E = (U/2 - t)$  over the ground state  $\textcircled{A}$ . As a result, at half-filling in the strong-coupling limit, the pairing attraction between top- and bottom-layer electrons  $V_{\text{eff}}$  in

the spinless model should in general scale like,

$$V_{\text{eff}} \propto -U. \quad (7)$$

In DQMC calculations at high temperatures, layer density fluctuations can prevail. Thus it is reasonable finding out a scaling of ,

$$V^* \sim U/2 \quad (8)$$

in DQMC, where  $V^*$  is the DQMC estimation of  $V_{\text{eff}}$  (see main text). At low temperatures, [or if the intra-layer nearest-neighbor (NN) repulsion  $U_{nn}$  is introduced], the layer density fluctuations  $\delta n_l$  can be suppressed, which may lead to a larger  $V_{\text{eff}}$

$$V_{\text{eff}} \sim U \quad (9)$$

Our low-temperature DMFT calculations show that robust Kohn-Luttinger pairing can persist even when  $U^* \gg U/2$  (Fig. 3b), which implies an effective interaction  $|V_{\text{eff}}| \gg U/2$ . This phenomenon likely stems from the suppression of density fluctuations, as discussed above. However, the contribution from retardation effects of pairing at large  $U^*$  cannot be ruled out. Further investigation is required to fully clarify this point.

In DQMC simulation, the pairing susceptibility  $\chi_{\ell}^{(\alpha, \beta)}$  is defined as,

$$\chi_{\ell}^{(\alpha, \beta)} = \frac{1}{N_s N_{\ell}} \sum_{i, j, a, b} \int_0^{\beta} d\tau \langle \mathcal{T}_{\tau} p_{j, a}^{\dagger \ell, (\alpha, \beta)}(\tau) p_{i, b}^{\ell, (\alpha, \beta)}(0) \rangle$$

here  $p_{i, b}^{\ell, (\alpha, \beta)}$  is the pairing operator for a pair of electrons located at sites  $i$  and  $i + b$ . For brevity, here we use composite index  $\alpha \equiv (m, \sigma)$  to label electron components. For a spin (layer) singlet/triplet pairing,  $p_{i, b}^{\ell, (\alpha, \beta)} = \frac{\sqrt{2}}{2} f_{i, b}^{\ell} (c_{i, \alpha} c_{i+b, \beta} \pm c_{i, \beta} c_{i+b, \alpha})$ , where  $f_{i, b}^{\ell}$  is the form factor in real space associated to specific pairing symmetry  $\ell$ .  $N_s$  denotes the number of sites, and  $N_{\ell} = \sum_b |f_{i, b}^{\ell}|^2$  is a renormalization factor.

Our DMFT calculations are based on a three-site effective impurity cluster representing a single unit cell (top-, middle-, and bottom- layer). The impurity model was solved using an open-source implementation of the continuous-time quantum Monte Carlo (CTQMC) method within the TRIQS 3.2 framework [67, 68], and the Hirsch-Fye quantum Monte Carlo impurity solver.

## ab initio Calculations

In the first principles density functional theory (DFT) calculations, we employed the Vienna Ab initio Simulation Package (VASP) [69, 70] and selected the Perdew-Burke-Ernzerhof (PBE) exchange-correlation functional [71] for structural relaxation and band structure calculations. To ensure a balance between calculation accuracy and efficiency, the plane-wave cutoff energy was set to 600 eV. The convergence criteria for electronic optimization and structural relaxation were strictly set to  $10^{-6}$  eV and 1 meV/Å respectively, to guarantee that the calculation results converge to a stable state. For the multi-layer system, we precisely controlled the inter-layer spacing and the thickness of the vacuum layer. The inter-layer spacing was fixed at 5 Å to simulate the inter-layer interactions in the actual system. Meanwhile, a 15 Å vacuum layer was set to effectively avoid interactions between periodic images and ensure the independence of the system. To more accurately describe the local properties of electrons in the system, we used DFT+ $U$  method with  $U = 3$  eV for Cr and  $U = 3.5$  eV for Fe [72, 73]. The WANNIER90 program [74, 75] was used to calculate maximally localized Wannier functions to create the low-energy Hamiltonian and the projection matrix. When computing the effective interaction matrix, we used the projection approach in conjunction with the constrained random phase approximation (cRPA) method [76]. This technique effectively describes the electron correlation effects in the system while being computationally efficient.

We calculated a series of 2D van der Waals materials and obtained their bare  $V$ , on-site Hubbard  $U_o$ , and the repulsion between electrons at neighboring layers  $U_{12} = U_{23} \equiv U$  (note that our conventions for  $U_o, U$  are slightly different from the usual definitions). As shown in Table I, P<sub>7/15</sub>Fe are Fe doped in 1 × 2 × 1 and 2 × 2 × 1 phosphorene supercell respectively. In the projected energy band, P<sub>01</sub> refers to the P atom adjacent to the doped atom. NaCr<sub>2</sub>Cl<sub>6</sub> is the adsorption of Na atom in the Cr<sub>2</sub>Cl<sub>6</sub> unit cell, as shown in Fig. 6. It is worth noting that the spin-polarized cases were calculated for P<sub>7/15</sub>Fe.

TABLE I. Bare  $V$ , Hubbard  $U_o$ , repulsion between electrons at neighboring layers  $U_{12}$ , orbitals, Energy window  $E_w$  for Wannier projection, and  $N_m$ . Here, the Fermi energy  $E_F$  is set to 0 and all the energy units are in eV.

Materials	$V$	$U_o$	$U_{12} \equiv U$	orbitals	$E_w$	$N_m$
Cr <sub>2</sub> I <sub>6</sub>	14.643	2.89	/	Cr( $d_{z^2}, d_{xy}, d_{x^2-y^2}$ )	[-0.48,0.52]	1
	15.04	2.86	0.33		[-0.48,0.52]	2
Cr <sub>2</sub> Br <sub>6</sub>	15.65	3.53	/	Cr( $d_{z^2}, d_{xy}, d_{x^2-y^2}$ )	[-0.643,0.857]	1
	16.12	3.72	0.45		[-0.643,0.857]	2
Cr <sub>2</sub> Cl <sub>6</sub>	16.36	4.23	/	Cr( $d_{z^2}, d_{xy}, d_{x^2-y^2}$ )	[-0.46,0.54]	1
	16.69	4.5	0.57		[-0.46,0.54]	2
P <sub>7</sub> Fe	3.38	0.742	/	P <sub>01</sub> ( $p_z, p_x$ )	[-1.85,0.65]	1
	4.1	0.684	0.152		[-1.91,1.09]	2
P <sub>15</sub> Fe	3.84	0.524	/	P <sub>01</sub> ( $p_z, p_x$ )	[-0.967,1.033]	1